Title of BS- MS Thesis

A thesis submitted towards partial fulfilment of
BS-MS Dual Degree Programme

by

Bhargava T

under the guidance of

Dr. T.S. Mahesh

Assistant Professor, IISER, Pune

Indian Institute of Science Education and Research
Pune

Certificate

This is to certify that this thesis entitled "ENTER TITLE HERE" submitted towards the partial fulfilment of the BS-MS dual degree programme at the Indian Institute of Science Education and Research Pune represents original research carried out by Bhargava T at Indian Institute of Science Education and Research, under the supervision of Dr. T.S. Mahesh, during the academic year 2012-2013.

Student
Bhargava T

Supervisor
Dr. T.S. Mahesh

Acknowledgements

The candidate would especially like to thank... <include all the necessary text here> .

Abstract

Decoherence is the process by which a quantum system interacts with its environment and evolves into an arbitrary state, often irreversible nonunitary evolution. This is a major setback for quantum information processing which requires the preservation of coherence in the system for implementation of quantum gates and also for storage of information (quantum memory). Dynamical decoupling is a well known technique to prevent the decoherence of open systems. We study the DD of multiqubit systems. Theory indicates that local control on each qubit (DD pulses at different times on each qubit) should perform better than global control (pulses at the same time). We observe that this is not the case in a two qubit system. We then come up with DD sequences based on the measured noise spectral density of the system and study its performance as compared to standard DD sequences acting locally and globally.

Contents

1 Introduction **4**

2 Theory **7**
2.1 NMR . . . 7
2.1.1 Overview . . . 7
2.1.2 Relaxation . . . 8
2.2 Decoherence Model . . . 9
2.3 Standard DD pulses . . . 10
2.3.1 CPMG . . . 10
2.3.2 UDD . . . 10
2.3.3 NUDD . . . 10
2.4 Filter Function . . . 11
2.4.1 Multiqubit Decoherence Control . . . 12
2.5 ODD theory . . . 13

3 Methods **15**
3.1 Global vs. Local control on $^{13}CHCl_3$ . . . 15
3.2 Studying different coherence orders . . . 15
3.2.1 Zero (double) Quantum Coherence . . . 16
3.2.2 Single Quantum Coherence . . . 17
3.3 Measuring the spectral densities . . . 18
3.3.1 Overview . . . 18
3.3.2 Extracting local and non-local spectral densities . . . 18
3.4 Optimisation . . . 19
3.5 Measuring the decay . . . 20

4 Results **21**
4.1 Global vs Local DD on $^{13}CHCl_3$ . . . 21
4.2 Extracting the Spectral Density . . . 21
4.3 Optimised Pulses . . . 22
4.4 Results obtained for different sequences . . . 22

5 Discussion **28**
5.1 Global vs. Local DD on $^{13}CHCl_3$ 28
5.2 Optimised DD 28

References **30**

A Long proofs **35**
A.1 Proof of the decoupling of the system from environment described in Sec. 2.2 35
A.2 Magnus Expansion 36
A.3 Nelder-Mead Optimisation 37
A.3.1 Overview 37
A.3.2 The algorithm 37

Chapter 1

Introduction

Quantum information processing uses quantum mechanical effects in systems to achieve information processing tasks [1]. It turns out that quantum computers are a necessity to study quantum systems. As Feynmann said about quantum computers, 'Nature isn't classical dammit, and if you want to make a simulation of nature, you'd better make it quantum mechanical, and by golly it's a wonderful problem because it doesn't look so easy.' [2] Since then, a lot of work has been done into designing and testing the working of several systems built to function like quantum computers. In 1996, S. Lloyd showed Feynmann's conjecture to be correct and showed that a quantum computer can simulate any quantum system accurately [3]. Since then, there has been a huge boom in the field, with several implementations of quantum computing springing up and huge progress in the development of a 'quantum computer'.

The conditions for a quantum computer were enlisted by Divincenzo [4] and clearly lay out the conditions necessary for a perfect system to behave like a perfect quantum computer. Several quantum systems have been demonstrated to satisfy several of these criteria, but to violate one or the other too. Systems such as optical cavities [5], ion traps [6, 7], Nuclear Magnetic Resonance (NMR)[8, 9, 10], Super quantum interfering device (SQUIDS)[11], nitrogen-vacancy centers [12] etc. have been widely used in the last two decades to achieve the implementation of quantum computational tasks.

The advantage a quantum computer has over its classical counterpart is it's ability to exist in a superposition. This allows the implementation of a function on several inputs at the same time. Several problems which lie in BQP (meaning the quantum computer can solve the problem in polynomial time, giving an erroneous output with at most 1/3 probability. This lies between P and PSPACE) are easily solvable using quantum computers. Some famous implementations of classical algorithms using quantum

computers are, the Shor's algorithm [13], implemented on a 7-qubit NMR system [14]. Several other such problems, such as the Grover's search algorithm [15, 16, 17, 18], finding discrete logarithms [13], quantum teleportation [19, 20], etc. have been implemented using quantum computers.

The use of NMR in the field of quantum information processing was suggested independently by Cory [10, 9]. The advantage of NMR as a tool for quantum computation is that, the measurement outcome is the expectation value of the observable, and not an eigenvalue [10]. The use of a certain manifold of the spin states is used in quantum computation, called the pseudo-pure states. However, there was a school of thought that believed that since liquid-state NMR didn't display any entanglement [21], and that it cannot be used for quantum information experiments. These claims were refuted by Laflamme et. al [22] who said that NMR system evolution is controlled by quantum mechanics, and must hence be useful for quantum simulations, and by saying that there was no proof that it was the appearance of entanglement that gave quantum computers their power. The NMR technology has so far proved to be an interesting and accessible technique to perform several QIP tasks [13] and that for small devices (small number of qubits), entanglement is not the most important resource. NMR is still arguably the most widely used implementation of QIP, though it is commonly accepted that it is not scalable to more than 15-20 qubits [10].

To implement efficient quantum computing, a qubit initiated in a particular state must remain in that state until quantum operations are performed on it, quantum entanglement between qubits must be sustained over time and exist as long no operations are performed. However, in reality, the system couples to its environment and this leads to the decay of the quantum state: the qubit, loses its coherence[23, 24, 25, 26].This process is called decoherence. This decoherence is one of the biggest hindrances in implementing quantum computation. Quoting Zurek, 'Above all, it (decoherence) is a threat to the quantumness of quantum information. It invalidates the quantum superposition principle, and thus turns quantum computers into (at best) classical computers, negating the potential power provided by the quantumness of the algorithms.' [27] Decoherence attacks the quantum entanglement, and this has been called early-stage disentanglement, or Entanglement Sudden Death [28]. The prevention of decoherence is thus a major hurdle in storing quantum memory, carrying out quantum operations, and quantum computing in general.

Several techniques have been implemented to counter decoherence. Dynamical decoupling [29] is one such technique built based on the spin echo technique [30]in NMR. The idea is that time independent couplings can be cancelled exactly by a π pulse exactly in the middle of the sequence. For

more complicated couplings, more involved pulse sequences like the CP [31] are designed. Several other techniques such as decoherence free subspaces, which attempt to identify states which don't decohere under a certain decoherence model [32]; quantum error correction codes [1]; some ideas based on the quantum zeno effect, where the state can be preserved by performing a series of fast projective measurements on the systems [33], etc. We basically want to optimise the sequences to yield maximum coherence and that is the objective of this thesis.

Chapter 2

Theory

2.1 NMR

2.1.1 Overview

Nuclear Magnetic Resonance (NMR) is basically based on the nuclear spin possessed by some isotopic forms of some nuclei. The spin of the nucleus gives rise to a magnetic moment, which in the presence of a strong magnetic field, precesses around this field. The relationship between the magnetic moment and the spin angular momentum operator ($\widehat{S}$) is $\widehat{\mu} = \gamma\widehat{S}$, where γ is the gyromagnetic ratio of the nucleus. In the presence of a magnetic field along, say, the Z direction, the nucleus precesses around the magnetic field (B_0) with an energy given by $\widehat{\mu}.\vec{B_0}$. The frequency of this rotation, called the Larmor Frequency, is thus given by $\omega_0 = \gamma B_0$. The precessing magnetic moments induce create a rotating magnetic field and a changing magnetic field creates an electric field which generates currents in the detector coils placed in the XY plane and if there exists a net magnetisation, this results in a electrical signal oscillating at the Larmor Frequency.
The Zeeman Hamiltonian of the system is thus given by $H_0 = \omega_0\widehat{I_z}$, and the state of the magnetization can be represented using the spin density operator. Using statistical mechanics the equilibrium density operator is found to be $\rho_{eq} = \frac{1}{2}\mathbb{I} + \frac{1}{2}\alpha\widehat{I_z}$ where $\alpha = \frac{(\hbar\gamma B_0)}{(K_B T)}$. We can then rotate the net magnetisation vector by applying radio frequency pulses to the sample. The flip angle (θ_p) is given by the product of the amplitude of the rf magnetic field (B_r) to the pulse time (τ_p), i.e, $\theta_p = -\gamma B_r \tau$. Hence a θ_x pulse rotates the magnetisation vector through an angle θ about the X axis.

2.1.2 Relaxation

Transverse Relaxation

A nucleus precessing about the B_0 magnetic field will also experience a local magnetic field because of the surrounding electrons and nuclei. This field is both a function of time and of the position of the nucleus. Hence, nuclei at different positions in the sample acquire different Larmor Frequencies and they slowly spread out in the XY plane eventually killing the net transverse magnetisation. This is similar to the case of several clocks started from the same position at the same instant, but running at different speeds. Eventually (after a time $\gg$ the time period of revolution ($\frac{1}{\omega_0}$), they will all point in various directions and the vector average of the position of all these clocks (corresponding to the magnetisation vector here), will be zero. The characteristic time for the net magnetisation to decay to 1/e of its initial value is called transverse relaxation time constant or spin-spin relaxation constant, T_2. This process of decay of the magnetisation vector is called decoherence and this is in general an irreversible process because of the time dependence of the local magnetic field experienced by a nucleus. The same process also occurs because of the inhomogeneity in the strong magnetic field. This process is called This inhomogeneity is constant in time and can be reversed by a process of 'spin echoes' as long as diffusion can be ignored in the relevant time scales.

Longitudinal Relaxation

As we have seen, there are small variations in the local magnetic field, in both the magnitude, and the direction. Hence the direction of precession changes with time. This is called 'wandering. This wandering is not isotropic. At non-zero temperatures, the spins seek a lower energy configuration as compared to higher energies. The direction parallel to the central magnetic field is the lowest energy state and hence the most preferred. Hence after a long time, at equilibrium, the net magnetisation points along the direction of the magnetic field. The time scale of this relaxation after any perturbation is of the order of T_1 also called the spin-lattice relaxation constant or the longitudinal relaxation constant. It is the time taken by the sample after the perturbation to relax to $(1 - e)$ times the equilibrium magnetisation.

$$M_z(t) = (1 - exp(\frac{t}{T_1}))M_{eq} \tag{2.1}$$

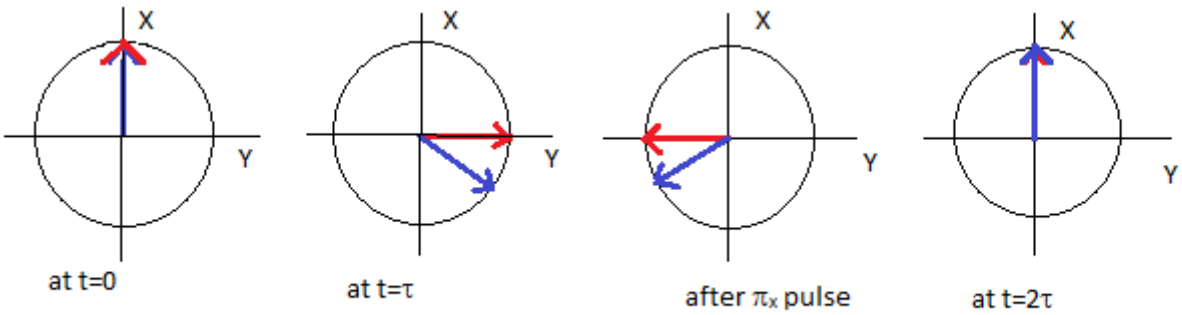

Figure 2.1: A simple illustration of the spin echo using two spins (red and blue arrows) which rotate at different frequencies.

Spin Echo

To refocus the magnetisation which has decayed because of the inhomogeneity in the longitudinal magnetic field, we use a technique called a Hahn echo to causing the re-emergence of the magnetisation. This basically involves a π_x after a time τ of evolution. This will give an 'echo', i.e, the transverse magnetisation re-emerges, at the end of another period of duration τ after the pulse (refer fig. 2.1.2).

2.2 Decoherence Model

We write the total Hamiltonian of the system and bath in the following manner. We write:

$$H = H_0 + H_{SB}, \quad H_0(t) = H_S + H_B \tag{2.2}$$

The von-Neumann equation thus reads:

$$\dot{\rho}_{tot}(t) = -i[H(t), \rho_{tot}(t)]; \hbar = 1 \tag{2.3}$$

$\rho_{tot}(t)$ is the density operator at time t, $H_S(t)$ is the system Hamiltonian, H_B is the Hamiltonian of the bath, and H_{SB} is the sytstem bath interaction Hamiltonian. The control of decoherence is achieved by a time dependent control Hamiltonian, $H_c(t)$ which acts on the system alone. The basic aim of the control pulses is to remove the interaction of the system with its bath, that is, ensure that the system doesn't evolve under the Hamiltonian H_{SB}. Refer to A.1 for the detailed derivation.

2.3 Standard DD pulses

There are several DD sequences in existence and new ones are constantly being designed for different purposes, with different advantages and drawbacks. (refer WDD, LODD, CDD [34],QDD [35],PDD (ref in J math phy 53, 122207) ....)

2.3.1 CPMG

The Carr-Purcell-Meiboom-Gill (CPMG) sequence (reference) is based on the CP sequence designed by Carr and Purcell in 1956(reference). This is based on the Hahn (spin) echo sequence, which consists of a $\left(\frac{\pi}{2}\right)_x - \tau - \pi_x - \tau$ sequence, which gives a re-emergence of the magnetisation at the end of the sequence. The CP sequence is basically a chain of π pulses of the form $\left(\frac{\pi}{2}\right)_x$ $(\tau - \pi_x - \tau)_n$. The CP pulse is however, not robust to errors in the π pulse. Given an error α in the pulse, the error at the end of n such pulses is given by $n\alpha$. To ensure robustness of these pulses, the CPMG pulses applied π pulses which were $\left(\frac{\pi}{2}\right)$ out of phase with the initial $\left(\frac{\pi}{2}\right)_x$ pulse. This ensures that any pulse error (α) will be cancelled out after every alternate π pulse and hence, there is no accumulation of errors. The sequence is thus,
$\left(\frac{\pi}{2}\right)_x$ $(\tau - \pi_y - \tau)_n$.

2.3.2 UDD

In 2007, Uhrig came up with the idea that an n-pulse sequence for time T with pulses at the time instants,

$$\delta_j = T sin^2 \left[\frac{\pi j}{2n+2}\right] \tag{2.4}$$

would perform better than any CPMG sequence. This was based on the filter function formalism in the next section (sec.2.4). He varied the parameters δ_j and made the first n derivatives of the filter function, $y_n(\omega t)|_{t=0}$ vanish. This gave him a sequence with pulses at the above time points, which achieves n^{th} order decoupling with n ideal π pulses. This DD sequence is called the Uhrig Dynamical Decoupling sequence.

2.3.3 NUDD

The Nested UDD (NUDD) sequence is a sequence which can tackle multi-qubit general decoherence.(reference j math phys 53, 122207) The UDD can

handle up to two-axis interactions, but its extension, the QDD (for single-qubit) and the NUDD (for multi-qubit), operate by nesting multi-layer UDD sequences. In this sequence, the n pulses on the 1st qubit are at time instants:

$$\delta_j = T sin^2 \left[\frac{\pi j}{2n+2} \right] \tag{2.5}$$

and the pulses on the 2nd qubit are at:

$$\delta_{jk} = (\delta_j - \delta_{j-1}) sin^2 \left[\frac{\pi k}{2n+2} \right] \tag{2.6}$$

This implies that between every two pulses on the 1st qubit, we have n pulses on the 2nd qubit. The total number of pulses in this sequence is therefor $n^2 + 2n$, n on the 1st qubit, and $n^2 + n$ on the 2nd. Refer to (j math....) for a universality proof of the NUDD sequence.

2.4 Filter Function

Uhrig has shown in (prl 98, 100504) that the decay of the signal in a thermal equilibrium spin which has been rotated into the transverse XY-plane is given as a function of the spectral density $S(\omega)$, i.e, the coupling of the bath to the environment; and a 'filter function', $y_n(\omega t)$.
He considers a bosonic bath coupling to the spin given by the hamiltonian:

$$H = \sum_i \omega_i b_i^\dagger b_i + \frac{1}{2} \sigma_z (b_i^\dagger + b_i) \tag{2.7}$$

The spin initially starts out in the eigenstate of the σ_z operator, denoted by $|\uparrow\rangle$, rotated by a $\pi/2$ pulse and then evolves under the Hamiltonian and is acted upon by the π-pulses. The signal which is basically the expectation value of σ_y is given by,

$$\begin{aligned} s(t) &= \langle \uparrow | D_x(\pi/2)^\dagger \tilde{R}^\dagger \sigma_y \tilde{R} D_x(\pi/2) | \uparrow \rangle \\ \tilde{R} &= D_y(\pi) exp(-iH(\delta_n - \delta_{n-1})t) D_y(\pi) exp(-iH(\delta_{n-1} - \delta_{n-2})t) .... D_y(\pi) exp(-iH\delta_1 t) \end{aligned} \tag{2.8}$$

where the $\delta_i t$s are the time instants at which the π-pulses are applied. The signal is found to be of the form,

$$
\begin{aligned}
s(t) &= cos[2\phi(t)]exp[-2\chi(t)] \\
\phi(t) &= \frac{1}{2}\int_0^\infty J(\omega)\frac{sin(\omega t)}{\omega^2}\,d\omega \\
\chi_n(t) &= \int_0^\infty J(\omega)\frac{|y_n(\omega t)|^2}{4\omega^2}coth(\beta\omega/2)\,d\omega \\
y_n(\omega t) &= 1 + (-1)^{n+1}e^{i\omega t} + 2\sum_{j=1}^{n}(-1)^j e^{i\omega t\delta_j}
\end{aligned}
\tag{2.9}
$$

We call the function $y_n(\omega t)$ the 'filter function' and use this filter function formalism to estimate the decay of coherence as a function of time.

2.4.1 Multiqubit Decoherence Control

Multiqubit decoherence is much more complicated to control than single-qubit decoherence, because of the fact that the entanglement between the qubits is very vulnerable to the environment and is quite easily destroyed (reference ESD papers). Also the qubits are coupled to each other and this *cross-decoherence* causes complications.
Similar to the filter function formalism for the one qubit case, Gordon et. al have come up with relations for multiqubit system. The decay of the signal $\chi(t)$ (refer section 2.4) is given now by a matrix as are the coupling matrix and the filter functions.

$$
\begin{aligned}
\chi_{jj'}(t) &= 2\pi\int_{-\infty}^{\infty} d\omega S_{jj'}(\omega)y_{jj'}(\omega t), \\
y_{jj'}(\omega t) &= y_j^*(\omega t)y_{j'}(\omega t)
\end{aligned}
\tag{2.10}
$$

From these equations and from figure 2.4.1, we can see that individually controlling each of the spins is advantageous as compared to a 'global' (identical) modulation. The cross decoherence term can be completely eliminated in this case, and we can see that that using different symmetry properties in the modulation control (Identically coupled particles (ICP), Independent Identical Particles (IIP), etc.), we can achieve good state preservation (refer kurizki work again).

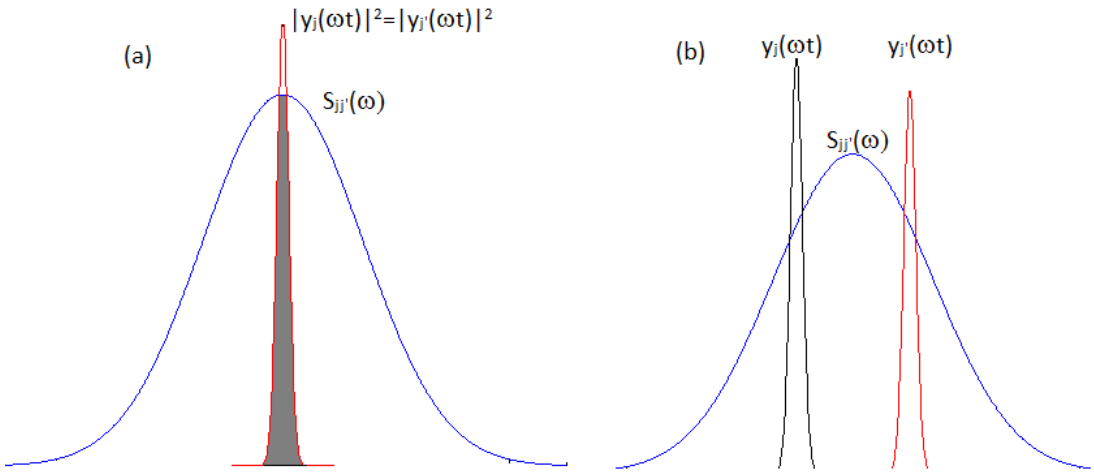

Figure 2.2: The spectral density function $S_{jj'}(\omega)$ and the filter function as a function of ω. In (a), the control functions are global and we can see have a maximum overlap (shaded) with the spectral density function resulting in non-zero $\chi(t)$. In (b), the two filter functions are disparate and hence cause minimal overlap in the cross-decoherence.

2.5 ODD theory

In this method based on the work of (reference j phys b 44 175501), we assume the two-qubit system is undergoing pure dephasing under the Hamiltonian,

$$H = f_1(t)\sigma_{z1} + f_2(t)\sigma_{z2} + f_3(t)\sigma_{z1}\sigma_{z2} \tag{2.11}$$

where $f_1(t)$ is the random time dependent noise on the first qubit alone, $f_2(t)$ is the noise on the 2nd qubit alone, and $f_3(t)$ is the component of the noise that affects both qubits. $f_1(t)$ and $f_2(t)$ are called the 'local' noises and $f_3(t)$ is called the 'non-local' noise. That is to say, $f_1(t)$ and $f_2(t)$ describe the interaction of each qubit with just their environment. The $f_3(t)$ term describes how qubit 1 (qubit 2) is also part of the environment of qubit 2 (qubit 1) and affects its dynamics. Given an initial state of the form $|\psi(0)\rangle = \alpha|\downarrow\downarrow\rangle + \beta|\downarrow\uparrow\rangle + \gamma|\uparrow\downarrow\rangle + \delta|\uparrow\uparrow\rangle$, it evolves under the Hamiltonian in eqn. 2.11 to

$$\begin{aligned}|\psi(t)\rangle =& \alpha e^{-i[-F_1(t)-F_2(t)+F_3(t)]}|\downarrow\downarrow\rangle + \beta e^{-i[-F_1(t)+F_2(t)-F_3(t)]}|\downarrow\uparrow\rangle \\ &+ \gamma e^{-i[F_1(t)-F_2(t)-F_3(t)]}|\downarrow\uparrow\rangle + \eta e^{-i[F_1(t)+F_2(t)+F_3(t)]}|\uparrow\uparrow\rangle\end{aligned} \tag{2.12}$$

where $F_i(t) = \int_0^t f_i(t')\,dt'$. In an ensemble of spins, initially in the state $|\psi(0)\rangle$, the density operator at any time t is given by,

$$\begin{aligned}\bar{\rho}_{01}(t) &= \alpha^*\beta\langle e^{-2i[F_2(t)-F_3(t)]^2}\rangle \\ &= \alpha^*\beta e^{-2[\langle F_2^2(t)\rangle+\langle F_3^2(t)\rangle]}\end{aligned} \tag{2.13}$$

with the other elements evolving similarly.
In the presence of the π pulses, the noise terms are modified to:

$$\begin{aligned}&\bar{F}_i(t) = \int_{-\infty}^{\infty} f_i(t')s_i(t')\,dt' \\ &s_i(t') = (-1)^{k_i}, t_{k_i} < t' \leq t_{(k_i+1)}, k_i = 0, 1, 2, ..., n_i \\ &n_1 = n, n_2 = m, n_3 = n + m\end{aligned} \tag{2.14}$$

where t_{k_1} are the time instants at which pulses are applied to qubit 1 and t_{k_2} are the time instants at which pulses are applied to qubit 2. The $s_i(t)$s are called the 'switch functions' and a pictorial understanding of this is provided in (reference biercuk's filter design paper). We then fourier transform to the frequency domain and find that the final averaged density operator is given by,

$$\bar{\rho}(t) = \begin{pmatrix} |\alpha|^2 & \alpha^*\beta e^{-\Gamma_2(t)-\Gamma_3(t)} & \alpha^*\gamma e^{-\Gamma_1(t)-\Gamma_3(t)} & \alpha^*\eta e^{-\Gamma_2(t)-\Gamma_1(t)} \\ \beta^*\alpha e^{-\Gamma_2(t)-\Gamma_3(t)} & |\beta|^2 & \beta^*\gamma e^{-\Gamma_2(t)-\Gamma_1(t)} & \beta^*\eta e^{-\Gamma_1(t)-\Gamma_3(t)} \\ \gamma^*\alpha e^{-\Gamma_1(t)-\Gamma_3(t)} & \gamma^*\beta e^{-\Gamma_2(t)-\Gamma_1(t)} & |\gamma|^2 & \gamma^*\eta e^{-\Gamma_2(t)-\Gamma_3(t)} \\ \eta^*\alpha e^{-\Gamma_2(t)-\Gamma_1(t)} & \eta^*\beta e^{-\Gamma_1(t)-\Gamma_3(t)} & \eta^*\gamma e^{-\Gamma_2(t)-\Gamma_3(t)} & |\eta|^2 \end{pmatrix} \tag{2.15}$$

where,

$$\begin{aligned}\Gamma_1 &= \int_0^{\infty} |y_n|^2 \frac{S_1(\omega)}{\omega^2}\,d\omega \\ \Gamma_2 &= \int_0^{\infty} |y_m|^2 \frac{S_2(\omega)}{\omega^2}\,d\omega \\ \Gamma_3 &= \int_0^{\infty} |y_{n+m}|^2 \frac{S_3(\omega}{\omega^2}\,d\omega\end{aligned} \tag{2.16}$$

where $y_i(\omega t)$ are the filter functions as defined in section 2.4.
Our aim is to maintain the state $\bar{\rho}(t)$ as close to the initial state $\rho(0)$ as possible. To this end, we define the fidelity between the two states as $C(t) = Tr[\bar{\rho}(t)\rho(0)]$ and wish to maximise this using the DD pulse. i.e, we wish to minimise $\phi(t) = 1 - C(t)$. This is then performed using the optimisation procedure described in section 3.4.

Chapter 3

Methods

3.1 Global vs. Local control on $^{13}CHCl_3$

We study the application of simple global (same number of π pulses on both spins, at the same instants) and local (different number of π pulses on each spin with the same total duration) on a two-qubit sample of labelled chloroform ($^{13}CHCl_3$). We measure the T_2 using the procedure illustrated in section 3.5. We perform six different experiments with a total evolution time T of 400ms. We look at the preservation of the double quantum coherence as entanglement is expected in terms of the form I_xS_x, etc.

1. No DD
2. 110 π pulses on only the ^1H spin
3. 110 π pulses on only the ^{13}C spin
4. 110 π pulses on both the ^1H spin and the ^{13}C spin
5. 110 π pulses on the ^1H spin and 99 π pulses on the ^{13}C spin
6. 99 π pulses on the ^1H spin and 110 π pulses on the ^{13}C spin

The pulse program was the same as that used in the double quantum coherence measurement in the optimisation experiment described below. (see figure 3.1).

3.2 Studying different coherence orders

We wish to study the preservation of magnetisation of different coherence orders on application of various DD pulses. To achieve this, we must be able

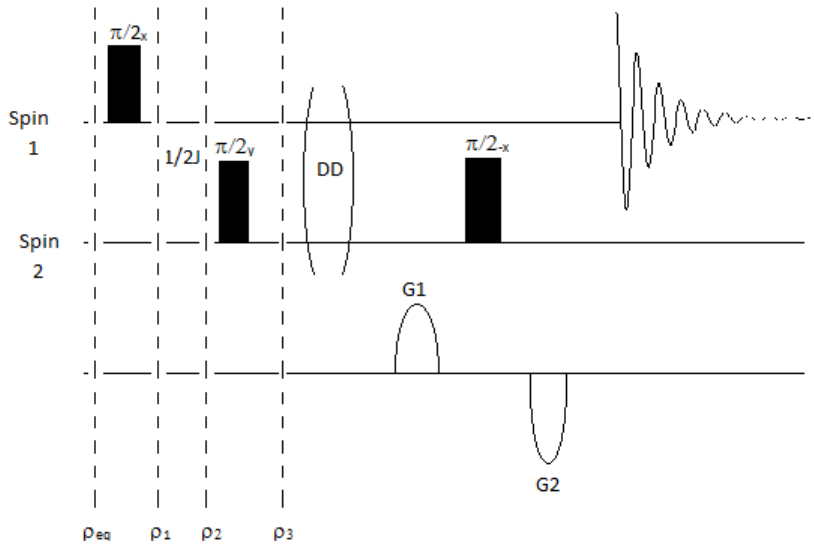

Figure 3.1: Pulse Program for detection of zero (double) quantum coherence

to destroy all coherences except for the one we want to observe, and convert this surviving coherence into a single quantum coherence (since this is the only coherence order which gives a non-zero signal in NMR).

3.2.1 Zero (double) Quantum Coherence

The pulse sequence used for detection of the zero (double) quantum coherence while destroying double (zero) and single quantum coherence is given in figure 3.1. We start out with the thermal equilibrium state, and the state at each point in the pulse program is as follows:

$$\begin{aligned} \rho_{eq} &= I_z + S_z \\ \rho_1 &= -I_y + S_z \\ \rho_2 &= -I_x S_z + S_z \\ \rho_3 &= -I_x S_x + S_x \end{aligned} \tag{3.1}$$

So, as we can see, we have effectively created a $I_x S_x$ term which contains both double and zero quantum coherence. We know that under the gradient, the evolution of the magnetisation is proportional to $G\omega$ where G is the magnitude of the gradient and ω is the oscillation frequency. The double (zero) quantum coherence, oscillates at a frequency equal to the sum (dif-

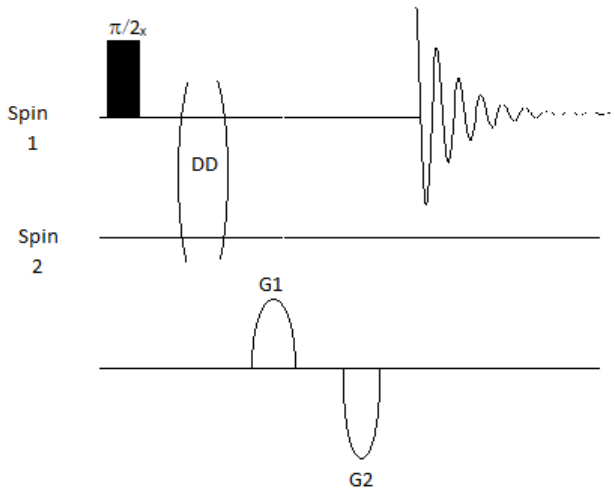

Figure 3.2: Pulse sequence to detect single quantum coherence

ference) of the larmor frequency of the individual spins. We hence use two gradients, $G_1 1$ and G_2. G_1 destroys all the magnetisations, irrespective of order. If we set G_2 to be of equal strength but in the opposite direction, for the same time as G_1, all the coherences would be refocussed. So, we convert the double (zero) quantum coherence into single quantum coherence so that the magnetisation we want to measure is now precessing like a single quantum coherence, and then tune the strength of the second gradient such that $G_1(\omega_I \pm \omega_S) = -G_2\omega_I$. This will refocus the double (zero) quantum coherence alone while destroying all others. The signal is then measured on the spin 1 channel.

3.2.2 Single Quantum Coherence

The pulse program used for the detection of the single quantum coherence while destroying the zero and double quantum coherences is given in figure 3.2. It does not involve the creation of other coherence orders, and the strength of the both the gradients remains the same (though they are in opposite directions). This sequence measures only the single quantum magnetisation on channel 1.

3.3 Measuring the spectral densities

3.3.1 Overview

We use a method proposed by T.Yugo, et al. and G. Alvarez, D. Suter independently [36, 37]. The method is based on the application of π pulses, forming a filter function (as defined in section **??**), we use the relationship between the coherence time of the system (T_2) and the filter function and spectral density to obtain the spectral density of the system. We basically used a CPMG sequence for this procedure. The filter function of a CPMG sequence is a sinc function with lobes far away from the center. So we approximate the CPMG sequence to have a filter function which is a delta at the appropriate frequency. The relation between the measured coherence time (T_2^L), and the spectral density is

$$\frac{1}{T_2^L} = \frac{4}{\pi^2} S(\frac{\pi}{2\tau}) \tag{3.2}$$

where τ is the time gap in the $(\tau - \pi - \tau)$ CPMG sequence. So we use different values of τ and probe the spectral density at different frequencies and fit a curve to the obtained plot.

3.3.2 Extracting local and non-local spectral densities

As mentioned in section 2.5, we separately require both the local and the non-local spectral densities for the optimisation. We achieve this by taking a sample of chloroform ($CHCl_3$). This consists of chloroform molecules with ^{12}C and ^{13}C in a ratio of their natural abundance. The ^{12}C atoms do not couple with the protons and give rise to a single peak in the proton spectrum. The ^{13}C atoms interact with the protons and give rise to two satellite peaks on either side of the main peak. We apply the CPMG sequence on the proton channel and measure the T_2 times for both the peaks separately. The decay of the main peak gives us the local spectral density of the proton since it has no other spin coupled to it. The decay of the satellite peaks gives us the total spectral density (cross spectral density) because of both the local and the non-local noise. We extract the non-local spectral density from the definition of the CSD:

$$S_{tot} = S_{lcl}^* S_{nlcl} \tag{3.3}$$

where the * indicates complex conjugate. The non-local spectral density of carbon is the complex conjugate of that of the non-local spectral density of hydrogen (see section **??**) and we get the cross spectral density of the carbon from the decay of the peaks in the carbon channel. We extract the

local spectral density of carbon in a procedure similar to the extraction of the non-local spectral density for proton. We now have the three spectral densities, S_{lclH}, S_{lclC}, S_{nonlcl} and use these to optimise the pulse sequence as given in the optimisation procedure in section 2.5.

3.4 Optimisation

As indicated in section 2.5, our aim is to find the sequence of pulses on the two qubits which minimises the error function, $\phi(t)$. This is done using the Nelder-Mead Optimisation described in section A.3. As the initial guess for the simplex, we take different standard DD sequences such as CPMG and UDD, and write a matlab program which uses the 'fminsearch' function which is based on the Nelder-Mead algorithm (refer appendix A.3), which yields the optimum pulse sequence. We wish to optimise the sequence for a total time T seconds. To this end, we devise a loop of ODD sequences, each with seven pulses, each lasting $\frac{T}{a}$ seconds, where a is the number of such loops we wish to wish to implement in the given time. So our fminsearch optimises the pulse sequence for $\frac{T}{a}$ seconds, which is repeated a times, and the performance of the sequence is monitored.
The initial state for the double quantum coherence is given by,

$$\rho(0) = \frac{1}{4}\mathbb{I}+\frac{1}{4}\begin{pmatrix} 0 & 0 & 0 & \alpha \\ 0 & 0 & 0 & 0 \\ 0 & 0 & 0 & 0 \\ \alpha & 0 & 0 & 0 \end{pmatrix} \tag{3.4}$$

where $\alpha = \frac{(\hbar\gamma B_0)}{(K_B T)}$.
The final state $\bar{\rho}(t)$ is given by

$$\bar{\rho}(t) = \begin{pmatrix} \frac{1}{4} & 0 & 0 & \alpha e^{-\Gamma_1-\Gamma_2} \\ 0 & \frac{1}{4} & 0 & 0 \\ 0 & 0 & \frac{1}{4} & 0 \\ \alpha e^{-\Gamma_1-Gamma_2} & 0 & 0 & \frac{1}{4} \end{pmatrix} \tag{3.5}$$

and the error function $\phi(t)$ is given by $\phi(t) = 3 - 8\frac{\hbar^2\omega^2}{K_B^2 T^2}e^{-2(\Gamma_1-\Gamma_2)}$.
Similarly, the state for the zero and single quantum coherences, and the error functions for each of these can be computed and optimisation performed.

3.5 Measuring the decay

The measurement of the FID in NMR is a destructive measurement, in that, after measurement of the FID, the magnetisation is lost. But we need to measure the intensity of the spectrum at different times and hence determine the decay constant of the magnetisation decay. To do this, we implement the above pulse program for a time $\frac{T}{a}$, measure the FID, then wait for a time $5T_1$ which will allow the magnetisation to return to its equilibrium value (refer section 2.1.2) and then run the same pulse program, but this time, with DD for a time $\frac{2T}{a}$, and again measure the FID, and repeat this process a times. We thus get the intensity of the signal at a points between the time 0 and T and calculate the value of T_2 for this particular DD by fitting an exponential decay.

Chapter 4

Results

4.1 Global vs Local DD on $^{13}CHCl_3$

As mentioned in section 3.1, we studied the global and the local application of CPMG pulses on a system of C-13 labelled chloroform $^{13}CHCl_3$). The experiments we performed are detailed in section 3.1 and the results are tabulated in table 4.1.

4.2 Extracting the Spectral Density

The proton and the ^{13}C spectrum of chloroform is shown in figure 4.2.

As detailed in section 3.3.2, we extract the spectral densities of Carbon-13 and Hydrogen by applying CPMG pulses to both the spins separately. The data is presented in figure 4.2.

We fit a gaussian to each of these spectral density curves and wind up with

Table 4.1: Global vs. Local Results

Type of DD	T_2 measured (in ms)
No DD	106.1
110 CPMG on ^1H only	152.7
110 CPMG on ^{13}C only	142.8
110 CPMG on both spins	362.8
110 CPMG on ^{13}C and 99 CPMG on ^1H	282.4
99 CPMG on ^{13}C and 110 CPMG on ^1H	287.8

Table 4.2: T_2 values of different coherence orders using different DD sequences (in ms).

Coherence Order ↓, Type of DD →	No DD	CPMG	CPMG Shifted	ODD
Zero Quantum Coherence	219.3	462.2	655.4	2897.7
Single Quantum Coherence	79.0	86.4	645.8	436.4
Double Quantum Coherence	160.0	492.1	273.0	613.7

the following forms:

$$\begin{aligned} S_{lclH}(\omega) &= 0.1205exp\left(-\frac{\omega}{165.1060}\right)^2 + .24 \\ S_{totH}(\omega) &= 0.0927exp\left(-\frac{\omega}{962.4859}\right)^2 + .3025 \\ S_{totC}(\omega) &= 0.2exp\left(-\frac{\omega}{1203.9}\right)^2 + 2.25 \end{aligned} \tag{4.1}$$

We then use this data to obtain the local and the non local spectral densities of proton and ^{13}C using the method detailed in section 3.3.2. (figs. 4.2 and 4.2). Since the nonlocal spectral densities are related by $S_{nlclC}(\omega) = S^*_{nlclH}(\omega)$ (refer section 2.4.1), we use the nonlocal and the total density of carbon to calculate the local spectral density of carbon-13, $S_{lclC}(\omega)$.

4.3 Optimised Pulses

Based on the spectral densities obtained in the previous section, we optimise the pulse sequence for seven pulses on each spin, for a time of 27.78ms for zero and single quantum coherence and 13.89ms for double quantum coherence as described in section 2.5. The pulse sequences for several standard DD sequences as well as that for ODD to preserve single quantum coherence is given in figure 4.3

4.4 Results obtained for different sequences

Using the above pulse sequences, we applied different DD sequences (CPMG, UDD, NUDD, ODD) on the system and observe the preservation of all three coherence orders. The results obtained are given in figure 4.4. The value of T2 obtained for each coherence order under different DD sequences is tabulated in table **??**.

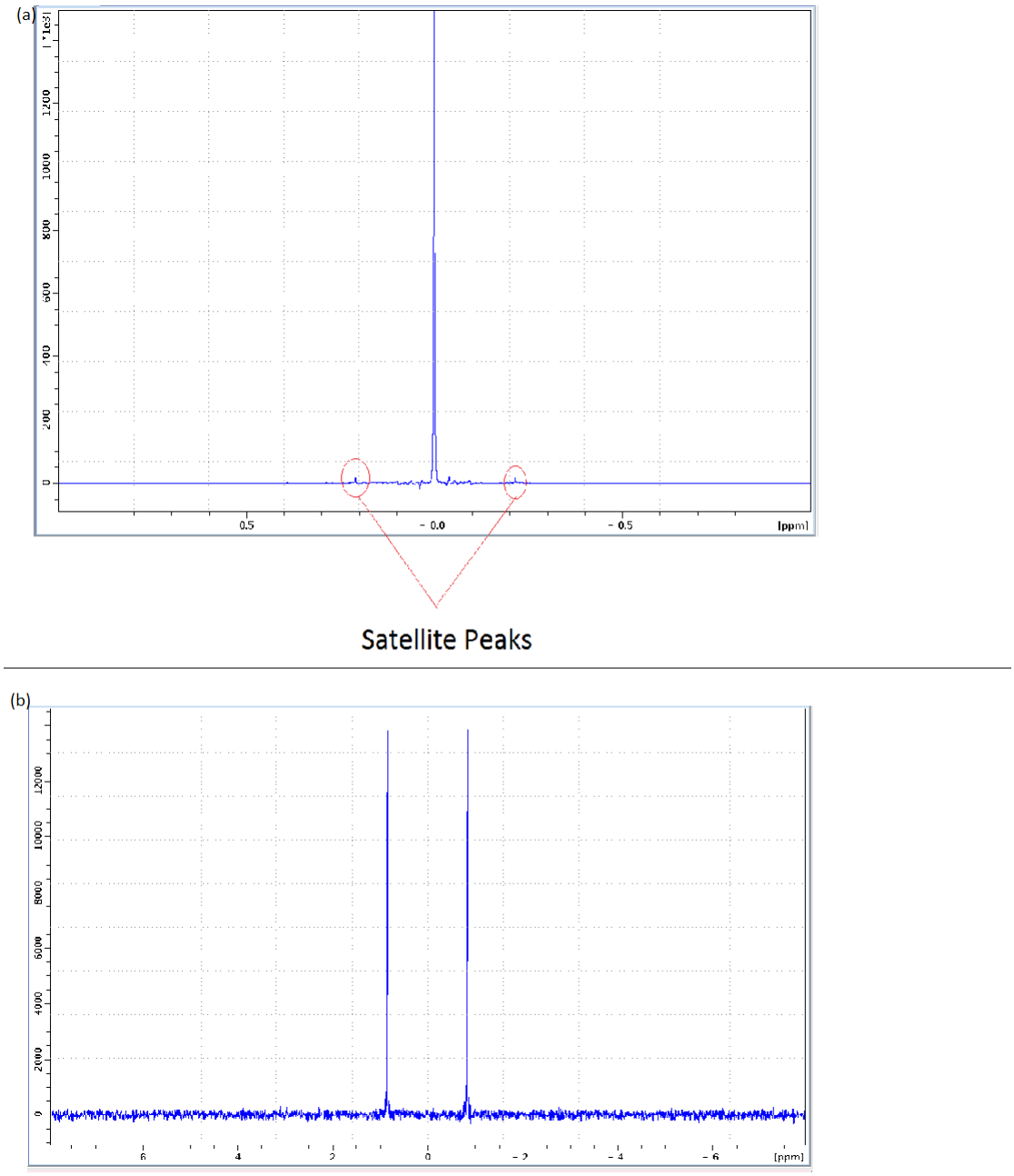

Figure 4.1: (a) The proton spectrum with the main peak due to the excess of $^{12}CHCl_3$ and the indicated J-coupled satellite peaks because of the natural abundance of $^{13}CHCl_3$ (b)J-coupled doublet C-13 spectrum.

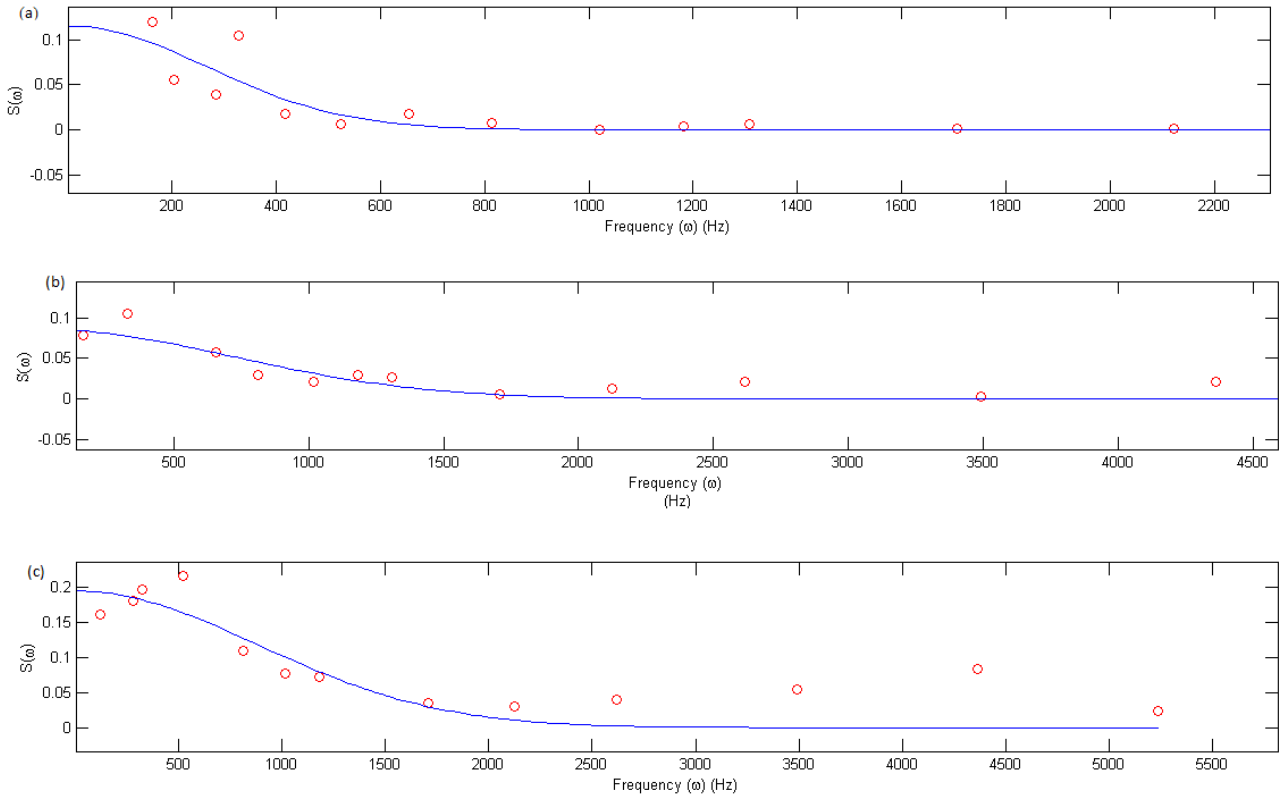

Figure 4.2: The spectral densities obtained (a) Local Spectral density of ^1H obtained from the central peak in the proton spectrum. (b) Total Spectral Density of ^1H obtained from the satellite peaks in the proton spectrum. (c) Total Spectral Density of ^{13}C obtained from the carbon spectrum.

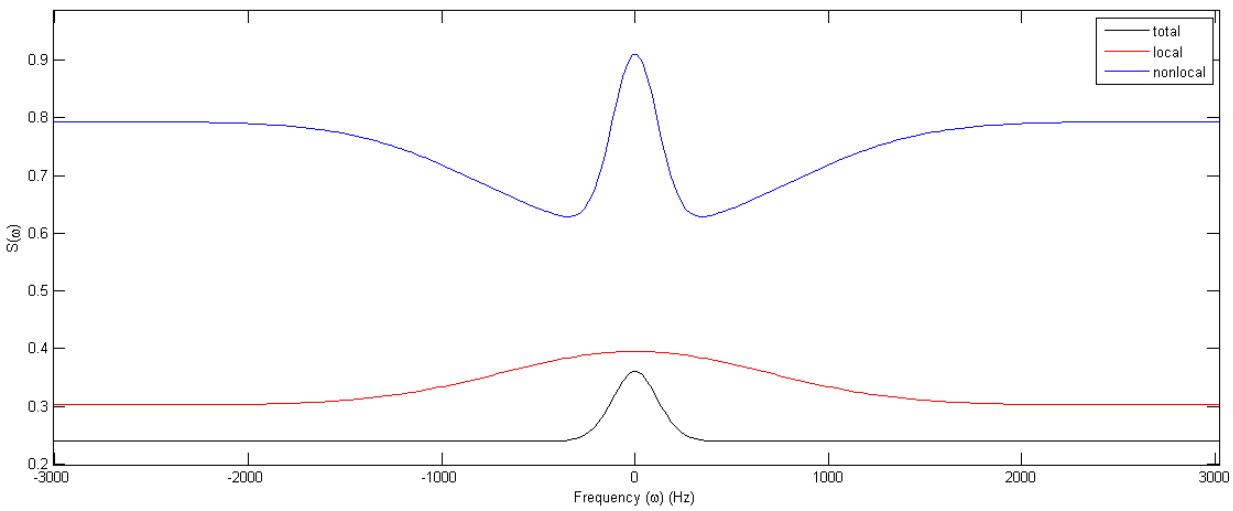

Figure 4.3: The black curve represents the total spectral density $S_{totH}(\omega)$, the red curve the local spectral density $S_{lclH}(\omega)$ and the blue curve, the derived nonlocal spectral density, $S_{nlclH}(\omega)$ (refer eqn. 4.1).

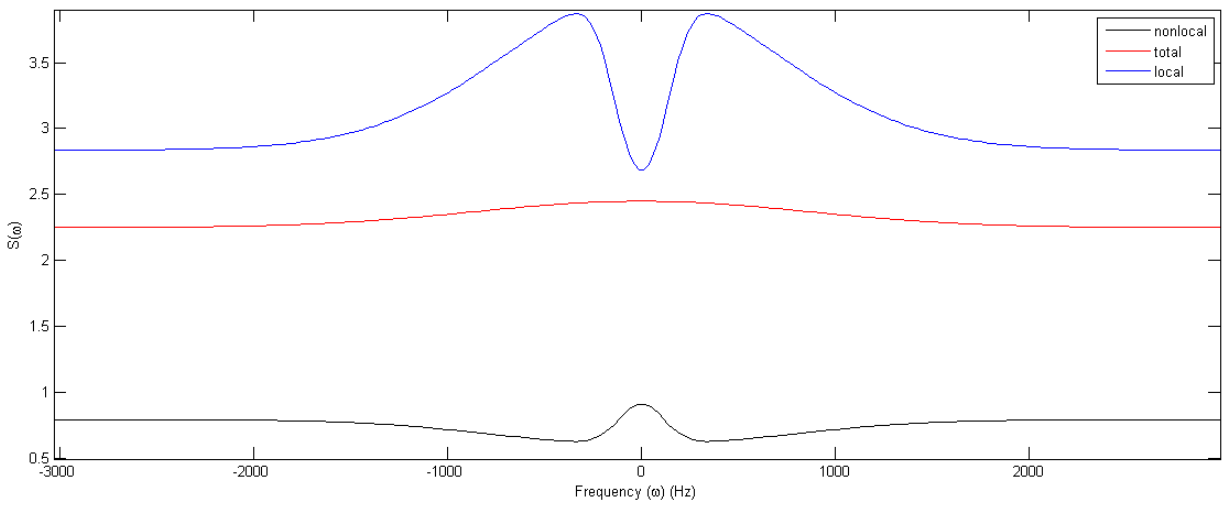

Figure 4.4: The black curve represents the nonlocal spectral density $S_{nlclC}(\omega)$, the red curve the total spectral density $S_{totC}(\omega)$ and the blue curve, the derived local spectral density, $S_{lclC}(\omega)$ (refer eqn. 4.1).

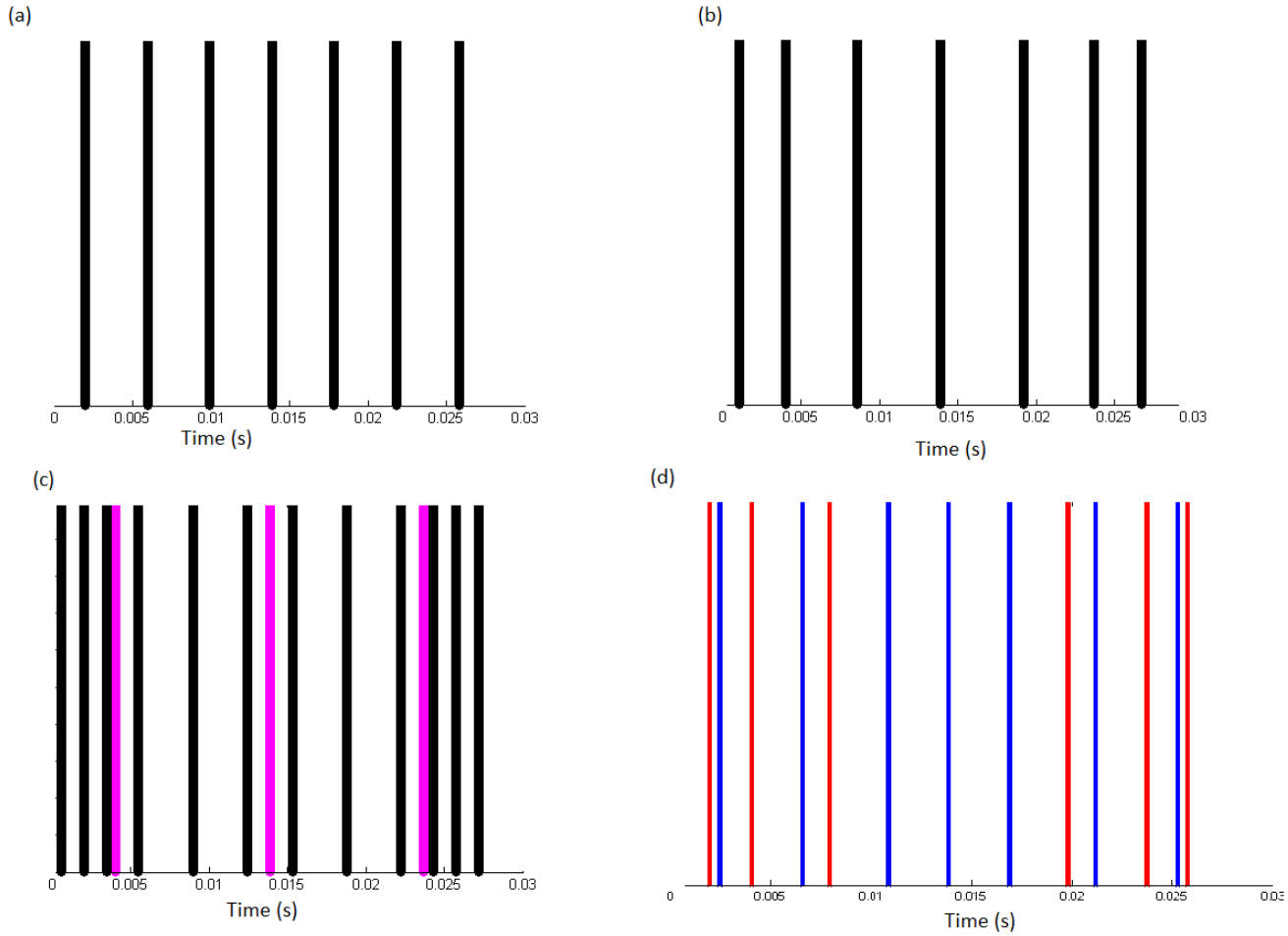

Figure 4.5: (a) pulse sequence for 7 CPMG pulses on both spins (b) Pulse sequence for 7 UDD pulses on both spins (c) pulse sequence for NUDD-3 (15 pulses). In a,b,c; the black lines represent pulse on spin 1, and the magenta lines represent pulses on spin 2. The two colours merge for CPMG and UDD on both. (d) The optimised pulse sequence for 7 pulses on each. The red colour indicates a pulse on spin 1, and a blue line, a pulse on spin 2. The central pulse (at t=13.89ms) is applied simultaneously on both spins.

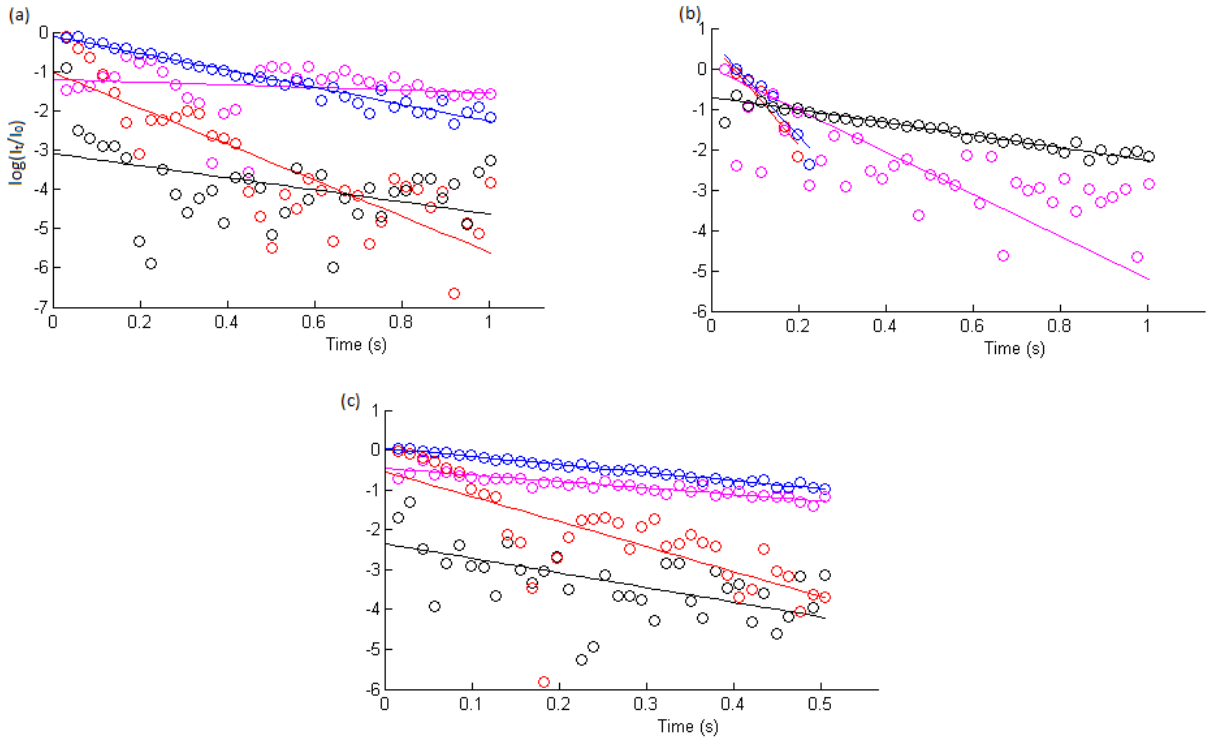

Figure 4.6: (a) Zero quantum data for a time T=1s, with seven pulses each on ^{13}C and ^{1}H in each time interval of 27.78ms. (b)Single quantum data for a time T=1s, with 7 pulses each on ^{13}C and ^{1}H in each time interval of 27.78ms. (c)Double quantum data for a time T=0.5s, with 7 pulses each on ^{13}C and ^{1}H in each time interval of 13.89ms. In all figures, the red line corresponds to No DD, the blue line corresponds to CPMG on both, magenta line to ODD and the black line to CPMG on the 2 shifted by a time τ.

Chapter 5

Discussion

5.1 Global vs. Local DD on $^{13}CHCl_3$

The results we obtained for the global vs. local DD experiment on $^{13}CHCl_3$ (refer to table 4.1)shows that a simultaneous CPMG sequence on both the spins is more effective in preserving the coherence of the system. This is contrary to what is expected because of the theory detailed in section 2.4.1 where we saw that the off-diagonal terms of the decoherence matrix (cross-decoherence terms) should vanish for local modulations (refer fig. **??**).

5.2 Optimised DD

The total spectral densities of both the ^{13}C and the ^{1}H spins and the local spectral density of the proton were obtained using the method outlined in section 3.3. Several functions including lorentzians were fitted to this data, and it was concluded that the spectral density most resembled a gaussian. We then used the method outlined in section 3.3.2 to obtain the non-local spectral density of the proton. The total spectral density and the local spectral density of the proton are both of the form $S(\omega) = aexp(-b/\omega)^2 + c$ and hence the non-local spectral density, which is obtained by dividing the total spectral density by the local spectral density is given in figure 4.2. The shape resembles that of a mexican wavelet which is described by the function $S(\omega) = \frac{2}{\sqrt{3\sigma}\pi^{1/4}}\left(1 - \frac{t^2}{\sigma^2}\right)e^{-\frac{t^2}{2\sigma^2}}$. The Mexican wavelet is a result of the difference between two gaussians. Using this non-local spectral density, which is the same for ^{13}C as well, we derive the local spectral density of the ^{13}C spin, and then optimise the pulses for DD. The optimised pulse sequence is shown in figure 4.3. The sequence is made symmetric with respect to time,

because this will ensure the refocussing of evolution due to any time independent noises. The sequence is quite evidently different from any of the other initial guesses and computational analysis shows that they minimise the error function (2.5) much better than any standard DD sequence.

In the experimental results, for all coherence orders, we see that there is some oscillation of the magnetisation measured. This is probably because of oscillation of the magnetisation between different coherence orders, and is not because of decoherence. To account for these oscillations, the data was fitted to an oscillating exponential decay, given by $aexp(-bt)(1+sin(ct+d))$. The decay of coherence is then given by the constant 'b' which is the inverse of the transverse relaxation time, T_2.

In all the coherence orders, it is quite obvious that decoherence sets in really quickly in the absence of any DD pulses (refer to the red lines in fig. 4.4). We see that in the presence of CPMG and ODD pulses, the coherence time is greatly improved in all coherence orders. ODD does have a marginal edge over CPMG. Especially in the case of double quantum coherence, which is what we would like to use to encode entanglement, etc., we see that ODD is quite efficient and preserves coherence for a long time. It is surprising to see that the single quantum coherence signal intensity decays almost as fast in the presence of CPMG as it does in the absence of any DD and so, we shifted the CPMG sequence on the 2nd spin by a time τ to ensure that this wasn't caused because of the interference of the two pulses, and this is the black line in all the figures.

So we can see that it is indeed to our advantage to design our dynamical decoupling pulses to fit the spectral density of the system we are working with. This will however be a problem in a general system, where we cannot use the method we used above to obtain the local and the non-local spectral densities. This optimisation method is also based on the initial state of the system on which you want to preserve coherence. Quite often, it happens to be the case that we do not know the state in which the system starts out and then the optimisation, averaging over all initial states, may not be quite as effective as when optimised for the specific state.

References

[1] M. Nielsen, I. Chuang, Quantum Computation and Quantum Information, Cambridge Series on Information and the Natural Sciences, Cambridge University Press, 2000.
URL http://books.google.co.in/books?id=65FqEKQOfP8C

[2] R. Feynman, P. W. Shor, Simulating physics with computers, SIAM Journal on Computing 26 (1982) 1484–1509.

[3] S. Lloyd, Universal quantum simulators, Science 273 (5278) (1996) 1073–1078. arXiv:http://www.sciencemag.org/content/273/5278/1073.full.pdf, doi:10.1126/science.273.5278.1073.
URL http://www.sciencemag.org/content/273/5278/1073.abstract

[4] D. P. DiVincenzo, Quantum computation, Science 270 (5234) (1995) 255–261. arXiv:http://www.sciencemag.org/content/270/5234/255.full.pdf, doi:10.1126/science.270.5234.255.
URL http://www.sciencemag.org/content/270/5234/255.abstract

[5] P. Grangier, G. Reymond, N. Schlosser, Implementations of quantum computing using cavity quantum electrodynamics schemes, Fortschritte der Physik 48 (9-11) (2000) 859–874. doi:10.1002/1521-3978(200009)48:9/11<859::AID-PROP859>3.0.CO;2-N.
URL http://dx.doi.org/10.1002/1521-3978(200009)48:9/11<859::AID-PROP859>3.0.CO;2-N

[6] W. Paul, H. Steinwedel, Ein neues Massenspektrometer ohne Magnetfeld, Zeitschrift Naturforschung Teil A 8 (1953) 448.

[7] J. I. Cirac, P. Zoller, Quantum computations with cold trapped ions, Phys. Rev. Lett. 74 (1995) 4091–4094. doi:10.1103/PhysRevLett.74.4091.
URL http://link.aps.org/doi/10.1103/PhysRevLett.74.4091

[8] W. S. Warren, The usefulness of nmr quantum computing, Science 277 (5332) (1997) 1688–1690. arXiv:http://www.sciencemag.org/content/277/5332/1688.full.pdf, doi:10.1126/science.277.5332.1688.
URL http://www.sciencemag.org/content/277/5332/1688.short

[9] N. A. Gershenfeld, I. L. Chuang, Bulk spin-resonance quantum computation, Science 275 (5298) (1997) 350–356. arXiv:http://www.sciencemag.org/content/275/5298/350.full.pdf, doi:10.1126/science.275.5298.350.
URL http://www.sciencemag.org/content/275/5298/350.abstract

[10] Ensemble quantum computing by nmr spectroscopy, in: Proc Natl Acad Sci U S A., Vol. 94(5).

[11] P. J. D. E. V Bouchiat, D Vio, M. H. Devoret, Quantum coherence with a single cooper pair, Phys. Scr. T76 (1) (1998) 165.
URL http://stacks.iop.org/1402-4896/1998/i=T76/a=024

[12] P. Neumann, N. Mizuochi, F. Rempp, P. Hemmer, H. Watanabe, S. Yamasaki, V. Jacques, T. Gaebel, F. Jelezko, J. Wrachtrup, Multipartite entanglement among single spins in diamond, Science 320 (5881) (2008) 1326–1329. arXiv:http://www.sciencemag.org/content/320/5881/1326.full.pdf, doi:10.1126/science.1157233.
URL http://www.sciencemag.org/content/320/5881/1326.abstract

[13] P. W. Shor, Polynomial-time algorithms for prime factorization and discrete logarithms on a quantum computerarXiv:quant-ph/9508027.

[14] G. B. C. S. Y. M. H. S. I. L. C. Lieven M.K.Vandersypen, Matthias Steffen, Experimental realization of shor's quantum factroing algorithm using nuclear magnetic resonance, Nature 414.

[15] L. K. Grover, Quantum computers can search arbitrarily large databases by a single query, Phys. Rev. Lett. 79 (1997) 4709–4712. doi:10.1103/PhysRevLett.79.4709.
URL http://link.aps.org/doi/10.1103/PhysRevLett.79.4709

[16] Z. J. Deng, L.-M. Liang, W. L. Yang, Scalable Implementation of Multiqubit Quantum Grover Search with Atomic Ensembles by Adiabatic Passage, International Journal of Theoretical Physics 49 (2010) 1904–1910. doi:10.1007/s10773-010-0374-6.

[17] X.-H. Zheng, P. Dong, Z.-Y. Xue, Z.-L. Cao, Implementation of the grover search algorithm with josephson charge qubits, Physica C: Superconductivity 453 (1ÃćâĆňâĂIJ2) (2007) 76 – 79. doi:10.1016/j.physc.2006.12.015.
URL http://www.sciencedirect.com/science/article/pii/S0921453406008756

[18] K.-A. Brickman, P. C. Haljan, P. J. Lee, M. Acton, L. Deslauriers, C. Monroe, Implementation of grover's quantum search algorithm in a scalable system, Phys. Rev. A 72 (2005) 050306. doi:10.1103/PhysRevA.72.050306.
URL http://link.aps.org/doi/10.1103/PhysRevA.72.050306

[19] C. H. Bennett, G. Brassard, C. Crépeau, R. Jozsa, A. Peres, W. K. Wootters, Teleporting an unknown quantum state via dual classical and einstein-podolsky-rosen channels, Phys. Rev. Lett. 70 (1993) 1895–1899. doi:10.1103/PhysRevLett.70.1895.
URL http://link.aps.org/doi/10.1103/PhysRevLett.70.1895

[20] T. S. D. W. S. K. W. N. B. W. A. M. J. K. E. A. V. M. T. J. R. U. A. Z. Xiao-Song Ma, Thomas Herbst, Quantum teleportation over 143 kilometres using active feed-forward, Nature 489 (2012) 269–273. doi:10.1103/PhysRevLett.70.1895.
URL http://dx.doi.org/10.1038/nature11472

[21] S. L. Braunstein, C. M. Caves, R. Jozsa, N. Linden, S. Popescu, R. Schack, Separability of very noisy mixed states and implications for nmr quantum computing, Phys. Rev. Lett. 83 (1999) 1054–1057. doi:10.1103/PhysRevLett.83.1054.
URL http://link.aps.org/doi/10.1103/PhysRevLett.83.1054

[22] R. Laflamme, D. G. Cory, C. Negrevergne, L. Viola, Nmr quantum information processing and entanglementarXiv:quant-ph/0110029.

[23] W. Dür, H.-J. Briegel, Stability of macroscopic entanglement under decoherence, Phys. Rev. Lett. 92 (2004) 180403. doi:10.1103/PhysRevLett.92.180403.
URL http://link.aps.org/doi/10.1103/PhysRevLett.92.180403

[24] C. Simon, J. Kempe, Robustness of multiparty entanglement, Phys. Rev. A 65 (2002) 052327. doi:10.1103/PhysRevA.65.052327.
URL http://link.aps.org/doi/10.1103/PhysRevA.65.052327

[25] T. Yu, J. H. Eberly, Phonon decoherence of quantum entanglement: robust and fragile states, Phys. Rev. B 66 (2002) 193306. doi:10.1103/PhysRevB.66.193306.
URL http://link.aps.org/doi/10.1103/PhysRevB.66.193306

[26] W. H. Zurek, Decoherence, einselection, and the quantum origins of the classical, Rev. Mod. Phys. 75 (2003) 715–775. doi:10.1103/RevModPhys.75.715.
URL http://link.aps.org/doi/10.1103/RevModPhys.75.715

[27] W. H. Zurek, Decoherence and the transition from quantum to classical, physicstoday 44 (1991) 36. doi:http://dx.doi.org/10.1063/1.881293.

[28] T. Yu, J. H. Eberly, Sudden death of entanglement, Science 323 (5914) (2009) 598–601. arXiv:http://www.sciencemag.org/content/323/5914/598.full.pdf, doi:10.1126/science.1167343.
URL http://www.sciencemag.org/content/323/5914/598.abstract

[29] L. Viola, S. Lloyd, Dynamical suppression of decoherence in two-state quantum systems, Phys. Rev. A 58 (1998) 2733–2744. doi:10.1103/PhysRevA.58.2733.
URL http://link.aps.org/doi/10.1103/PhysRevA.58.2733

[30] E. L. Hahn, Spin echoes, Phys. Rev. 80 (1950) 580–594. doi:10.1103/PhysRev.80.580.
URL http://link.aps.org/doi/10.1103/PhysRev.80.580

[31] H. Y. Carr, E. M. Purcell, Effects of diffusion on free precession in nuclear magnetic resonance experiments, Phys. Rev. 94 (1954) 630–638. doi:10.1103/PhysRev.94.630.
URL http://link.aps.org/doi/10.1103/PhysRev.94.630

[32] K.-A. S. G. Massimo Palma, A. K. Ekert, Quantum computers and dissipation, Vol. 452, 1996, pp. 567–584.

[33] B. Misra, E. C. G. Sudarshan, The zeno's paradox in quantum theory, J. Math. Phys. 18 (1977) 756. doi:http://dx.doi.org/10.1063/1.523304.

[34] K. Khodjasteh, D. A. Lidar, Fault-tolerant quantum dynamical decoupling, Phys. Rev. Lett. 95 (2005) 180501. doi:10.1103/PhysRevLett.

95.180501.
URL http://link.aps.org/doi/10.1103/PhysRevLett.95.180501

[35] J. R. West, B. H. Fong, D. A. Lidar, Near-optimal dynamical decoupling of a qubit, Phys. Rev. Lett. 104 (2010) 130501. doi:10.1103/PhysRevLett.104.130501.
URL http://link.aps.org/doi/10.1103/PhysRevLett.104.130501

[36] T. Yuge, S. Sasaki, Y. Hirayama, Measurement of the noise spectrum using a multiple-pulse sequence, Phys. Rev. Lett. 107 (2011) 170504. doi:10.1103/PhysRevLett.107.170504.
URL http://link.aps.org/doi/10.1103/PhysRevLett.107.170504

[37] G. A. Álvarez, D. Suter, Measuring the spectrum of colored noise by dynamical decoupling, Phys. Rev. Lett. 107 (2011) 230501. doi:10.1103/PhysRevLett.107.230501.
URL http://link.aps.org/doi/10.1103/PhysRevLett.107.230501

Appendix A

Long proofs

A.1 Proof of the decoupling of the system from environment described in Sec. 2.2

Moving to the interaction picture with $H_c(t)$ as the unperturbed Hamiltonian, the system-environment state evolves under the time-evolution operator:

$$\begin{aligned} &\tilde{U}_{tot}(t) = \mathcal{T}exp[-i\int_0^t \tilde{H}(s)\,ds] \\ &\tilde{H}(s) = U_c^\dagger(s)HU_c(s), \qquad\qquad U_c(t) = \mathcal{T}exp[-i\int_0^t H_c(s)\,ds] \end{aligned} \tag{A.1}$$

where the tilde represents operators in the interaction picture and the absence of tilde represents operators in the Schrödinger's picture.
We design the control Hamiltonian $H_c(t)$ such that,

$$\begin{aligned} &U_c(t+\tau) = U_c(t) \\ &\int_0^\tau dt[U_c^\dagger(t)H_{SB}U_c(t)] = 0 \end{aligned} \tag{A.2}$$

At $t = N\tau$, the state evolves with,

$$\begin{aligned} U_{tot}(N\tau) &= \mathcal{T}exp[-i\int_0^{N\tau} \tilde{H}(s)\,ds] \\ &= [\mathcal{T}exp(-i\int_0^\tau \tilde{H}(s)\,ds)]^N \end{aligned} \tag{A.3}$$

Using the magnus expansion (refer appendix A.2),

$$\tilde{U}_{tot}(\tau) = exp[-i\tau(\bar{H}^{(0)} + \bar{H}^{(1)} + ...)] \tag{A.4}$$

We ignore the higher order terms of the expansion because $H^{(k)}(t)$ goes as $\mathcal{O}(\tau^k)$ and for very small $\tau(\tau \to 0)$, the higher order terms are negligible.

$$\bar{H}^{(0)} = \frac{1}{\tau}\int_0^\tau \tilde{H}(s)\,ds \tag{A.5}$$

Using equation A.2, we get,

$$\bar{H}^{(0)} = \frac{1}{\tau}\int_0^\tau ds U_c^\dagger(s) H_0 U_c(s) \tag{A.6}$$

The evolution operator for the total time $t = N\tau$ is given by,

$$\begin{aligned} \tilde{U}_{tot}(N\tau) &= exp(-i(H'_S + H_B)t), \\ H'_S &= \frac{1}{\tau}\int_0^\tau dt U_c^\dagger(t) H_S U_c(t) \end{aligned} \tag{A.7}$$

Transforming back to the Schrödinger picture, we get

$$U_{tot}(t) = U_c(t) e^{-iH'_S t} e^{-iH_B t} \tag{A.8}$$

and for $t = N\tau$, $U_c(t) = U_c(0) = \mathbb{I}$.
So, we see that the system-bath coupling has been eliminated by the application of a fast control ($\tau \to 0$).

A.2 Magnus Expansion

The magnus expansion is used to find the time ordered exponential of a time dependent function.
When $Y(t) = \mathcal{T}exp(\int_{t_0}^t A(s)\,ds)Y(t_0)$, we define $\Omega(t, t_0) = \int_{t_0}^t A(s)\,ds$ and the function $\Omega(t, t_0)$ can be expanded as a series expansion, $\Omega(t, t_0) = \sum_{i=0}^{\infty} \Omega^{(k)}(t)$, where the first three terms are,

$$\begin{aligned} \Omega^{(0)}(t) &= \int_0^t A(s)\,ds \\ \Omega^{(1)}(t) &= \frac{1}{2}\int_0^t dt_1 \int_0^{t_1} dt_2 [A(t_1), A(t_2)] \\ \Omega^{(3)}(t) &= \frac{1}{6}\int_0^t dt_1 \int_0^{t_1} dt_2 \int_0^{t_2} dt_3([A(t_1), [A(t_2), A(t_3)]] + [A(t_3), [A(t_1), A(t_2)]]) \end{aligned} \tag{A.9}$$

A.3 Nelder-Mead Optimisation

A.3.1 Overview

This method finds the local minimum of a function $f(x_1, x_2, x_3, ...x_N)$of N parameters. It uses the concept of simplices. A simplex is a polytope of N+1 vertices in an N dimensional space. A polytope is a geometric object with flat sides. A polygon is a polytope in 2D, a polyhedron in 3D and so on. A simplex is thus a line segment in 1D, a triangle in 2D, a tetrahedron in 3D and so on. The objective of the algorithm is to find the vertex x_i which has the least value of $f(x_i)$. There are several variants of the Nelder-Mead optimisation and one such is described below.

A.3.2 The algorithm

The algorithm is as follows:

1 We construct a guess simplex with N+1 random vertices.

2 Order the vertices according to their functional values at that point, such that:
$f(x_0) \leq f(x_1) \leq f(x_2 \leq ..... \leq f(x_N)$

3 Compute the center of gravity (centroid) (x_0) of all the vertices except x_N.

4 **Reflection**

- Reflect the point x_N about the centroid, i.e $x_r = x_0 + \alpha(x_N - x_0)$
- If $f(x_0) \leq f(x_r) < f(x_{N-1})$, then replace x_N with x_r, go back to step 2.

5 **Expansion**

- If $f(x_r) < f(x_0)$, compute the expanded point $x_e = x_0 + \gamma(x_r - x_0)$
- If $f(x_e) < f(x_r)$, replace x_N with x_e, go back to step 2.
- If $f(x_e) \geq f(x_r)$, replace x_N with x_r, go back to step 2.

6 **Contraction**

- If $f(x_r) \geq f(x_{N-1})$, compute $x_c = x_0 + \rho(x_r - x_0)$.
- If $f(x_c) < f(x_N)$, replace x_N with x_c, go back to step 2.

7 **Reduction**
$x_i = x_i + \sigma(x_i - x_0)$ for all $i\epsilon 1, 2, 3, ..., N$, go back to step 2.

The values of $\alpha, \gamma, \sigma, \rho$ are fixed while defining the algorithm.
The initial guess simplex is important in that, if too small, the search is confined to a very small area in the parameter space and will wind up doing a local search.
The search progressively converges until all the vertices of the simplex converge to the local minimum.